Microchimica Acta (2024) 191:127
https://doi.org/10.1007/s00604-024-06204-8

ORIGINAL PAPER

Core–shell "loading-type" nanomaterials enabling glucometer readout for portable and sensitive detection of p-aminophenol in real samples

Xiang-Ling Li[1,2] · Lei Zhao[1,2] · Zi-Heng Wang[1,2] · Tian-Shun Song[1,2] · Ting Guo[3] · Jing Jing Xie[1,2]

Received: 12 October 2023 / Accepted: 8 January 2024 / Published online: 9 February 2024

Abstract

A one-target-many-trigger signal model sensing strategy is proposed for quickly, sensitive and on-site detection of the environmental pollutant p-aminophenol (PAP) by use of a commercial personal glucose meter (PGM) for signal readout with the core–shell "loading-type" nanomaterial MSNs@MnO_2 as amplifiable nanoprobes. In this design, the mesoporous silica nanoparticles (MSNs) nanocontainer with entrapped signal molecule glucose is coated with redoxable manganese dioxide (MnO_2) nanosheets to form the amplifiable nanoprobes (Glu-MSNs@MnO_2). When encountered with PAP, the redox reaction between the MnO_2 and PAP can induce the degradation of the outer layer of MSNs@MnO_2, liberating multiple copies of the loaded glucose to light up the PGM signal. Owing to the high loading capability of nanocarriers, a "one-to-many" relationship exists between the target and the signal molecule glucose, which can generate adequate signal outputs to achieve the requirement of on-site determination of environmental pollutants. Taking advantage of this amplification mode, the developed PAP assay owns a dynamic linear range of 10.0–400 μM with a detection limit of 2.78 μM and provides good practical application performance with above 96.7 ± 4.83% recovery in environmental water and soil samples. Therefore, the PGM-based amplifiable sensor for PAP proposed can accommodate these requirements of environment monitoring and has promising potential for evaluating pollutants in real environmental samples.

Keywords Core–shell · "Loading-type" nanomaterials; MnO_2 nanosheets · Amplifiable nanoprobes · PAP, On-site detection

Introduction

P-aminophenol (PAP), as a kind of aromatic pollutants, has a serious side effect to the environment and human health due to its intrinsic properties, such as long-term migration, difficult degradation, high toxicity, and easy bioaccumulation [1–6]; therefore, monitoring the aromatic pollutant PAP in our living environment (air, water, soil) is always a hot research topic, especially on-site detection.

Nowadays, various methods have developed to achieve sensitive detection of PAP, including high-performance liquid chromatography (HPLC) with diode array detection [7], gas chromatography-mass spectrometry (GC–MS) [8], electrochemical sensors with nanomaterials modified electrode such as hybrid material N-doped carbon dots decorated with manganese oxide nanospheres [9], Fe_3O_4@Au/MOF metal–organic framework nanoparticle [10], iodine/iodide-doped polymeric nanospheres [11], modified microchips-electrochemical [12], fluorescence methods based on nanoprobe 3D Eu(III) metal–organic framework [13], silica-coated CdTe quantum dots [14], and microchip electrophoresis with capacitively coupled contactless conductivity detection [15]. Although these methods are sensitive, their practical application is greatly limited by the complexity of the instruments and the need for skilled operators, as well as the time-consuming pre-treatment of samples, especially for home-style or on-site scenes.

✉ Ting Guo
guoting@hotmail.com

✉ Jing Jing Xie
xiej@njtech.edu.cn

1 State Key Laboratory of Materials-Oriented Chemical Engineering, Nanjing Tech University, Nanjing 211816, People's Republic of China

2 College of Biotechnology and Pharmaceutical Engineering, Nanjing Tech University, Nanjing 211816, People's Republic of China

3 Jiangsu Academy of Agricultural Sciences, Nanjing 210014, People's Republic of China

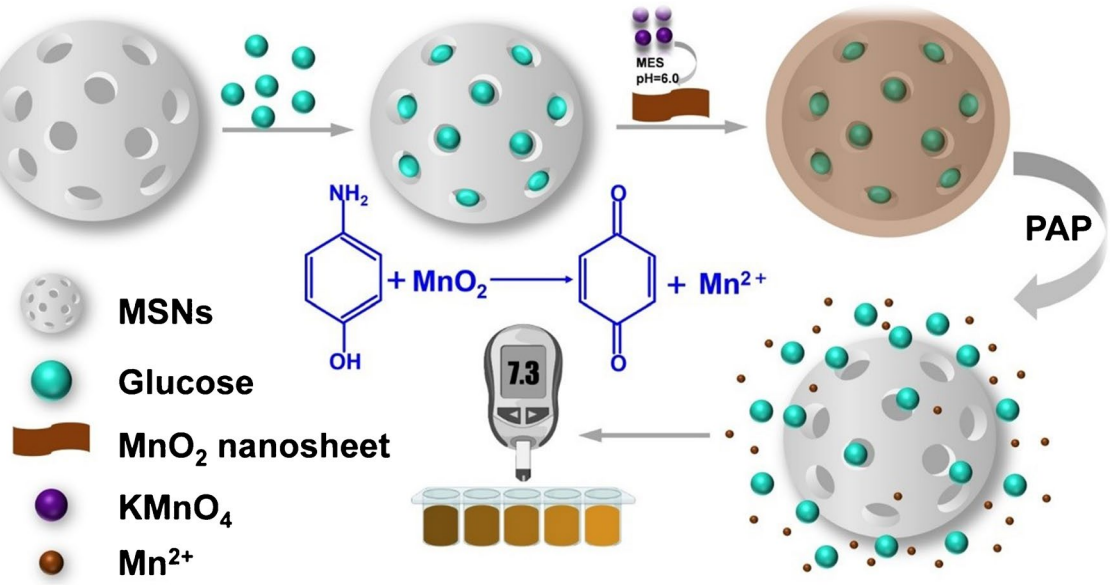

Scheme 1 Schematic illustration of one-target-many-trigger signal model sensing strategy for on-site detection of the aromatic pollutant PAP via the amplifiable nanoprobes Glu-MSNs@MnO_2

Driven by these issues and needs, several portable devices that can be easily accessible to end users have been developed, such as personal glucose meter (PGM), pressure gauges, and thermometers [16]. PGM is an extensively utilized personal diagnosis device for point-of-care testing. Due to its advantages such as pocket size, low cost, easy operation, and reliable quantitative result [17–19] as well as the rational design of the relationship between target recognition and glucose generation, PGM has been exploited for a variety of non-glucose targets analytes [20], including metal ions [21], nucleic acids [22, 23], small molecules [24–27], protein biomarkers [28, 29], etc. However, at the same time, we must be aware that the rapid on-site analysis via PGM, where the result read-out is based on one-target-one-trigger signal model, is still developing with problems remaining. Most traditional nanoprobe based on "one-to-one" signal model always generate too low signal change to meet the sensitivity of rapid on-site detection [30, 31].

And a series of amplification strategies, especially isothermal nucleic acid amplification methods, have been integrated with PGM detection to construct "one-to-many" signal model and achieve the effective sensitivity for on-site detection, whereas the whole sample-in-answer-out detection process of most such strategies still requires a longtime operation (nearly 1–2 h) which is not suitable for rapid on-site detection. Obviously, achieving new signal amplification strategies becomes one of the core tasks in the development of on-site detection. Nanoprobes as the cornerstone of detection process is a key element for achieving signal amplification. More recently, mesoporous silica nanoparticles (MSNs) as a type of loading nanomaterials have successfully integrated biorecognition unit, signal amplification unit, and carrier unit all-in-one to construct such nanoprobes, which have achieved effective "one-to-many" signal amplification and sensitive detection [32, 33]. Therefore, the combination of the "loading-type" nanomaterial as nanoprobes and the PGM as signal-readout device will accommodate this requirement and provide new directions to trace low abundance of environmental pollutants on-site.

Herein, we proposed a one-target-many-trigger signal model sensing strategy for rapid on-site detection of the environmental pollutant p-aminophenol (PAP), which used a commercial PGM for signal readout and the core–shell "loading-type" nanomaterials MSNs@MnO_2 as amplifiable nanoprobes (Scheme 1). Specifically, the MSNs entrapped signal molecule glucose is coated with a redoxable manganese dioxide (MnO_2) nanosheet to form the amplifiable nanoprobe. When encountered with PAP, the redox reaction between the layer MnO_2 and PAP induces the degradation of the outer layer of Glu-MSNs@MnO_2, liberating multiple copies of the loaded glucose to light up the PGM signal. Owing to the high loading capability of nanocarrier, a "one-to-many" relationship exists between the target and the signal molecule glucose, which can generate adequate signal outputs to achieve the requirement of on-site analysis of environmental pollutant.

Experimental section

Reagents

Sodium hydroxide (NaOH), potassium permanganate ($KMnO_4$), p-aminophenol (PAP), methyl ethanesulfonate (MES), potassium dihydrogen phosphate (KH_2PO_4), dipotassium hydrogen phosphate trihydrate (K_2HPO_4), and glucose were purchased from Sinopharm Chemical Reagent Co. Ltd.; 4-aminobenzenesulfonic acid, 4-aminobenzoic acid, diphenylamine, N-phenyl-1-naphthylamine, ethyl orthosilicate (TEOS), 3-aminopropyltriethoxysilane (APTES), and cetyltrimethylammonium bromide (CTAB) were purchased from J&K Scientific Co. All the chemicals were analytical grade and used without further purification.

Instruments

The UV–Vis measurements were performed on UV spectrophotometer UV-1900i (Shimadzu, Japan). All glucose levels were recorded by a personal glucose meter (Performa, ROCHE, Germany). The pH values were obtained by a PHS-3C pH meter (Leici, China). The N_2 adsorption–desorption isotherm was measured on Auto-sorb-iQA3200-4 (Quanta Tech Co., USA). The nanomaterials were characterized by JEM-2100 F Transmission Electron Microscope (Jeol, Japan).

Synthesis of MSNs and Glu-MSNs@MnO_2 nanomaterials

The MSNs were synthesized according to the previous research work with minor modification [34]. Specifically, CTAB (208 mg, 5.7×10^{-4} mol) was dissolved in 100 mL pure water and was gently stirred at 600 rpm to clarification; then, 0.725 mL of 1 M NaOH was added. The reaction solution was heated to 95 ℃, and TEOS (1.04 mL, 4.67×10^{-3} mol) was dropwise added to the above solution and then reacted for 2 h. After cooling, a milky white flocculent was obtained; then, the product was centrifuged at 8000 rpm for 3 min to remove excess reagents, and the residue was washed three times with pure water and ethanol respectively. The precipitate was dried in a vacuum oven at 60 ℃ for 10 h and was further calcined in a muffle furnace at 550 ℃ for 6 h to remove the surfactant template for obtaining the desired mesoporous nanomaterials (MSNs).

In order to prepare the amplifiable nanoprobe Glu-MSNs@MnO_2, 450 mg of glucose was dissolved in 5 mL of pure water, 20 mg of MSNs was added and ultrasonically dispersed in the glucose solution, and then, the solution was kept gently stirred at 600 rpm for 18 h to achieve the maximum loading efficiency. After loading process, the shell MnO_2 nanosheets was synthesized in situ. Specifically, 97.6 mg of MES and 3.95 mg of $KMnO_4$ were added to the above Glu-MSNs solution and ultrasonicated for 30 min; when the solution turned brown, it illustrated that the outer layer MnO_2 was successfully formed. Finally, the product was centrifuged at 6000 rpm for 2 min, and the residue was washed thoroughly with deionized water and redispersed in 2.5 mL buffer solution to obtain the nanoprobe Glu-MSNs@MnO_2 nanoprobes.

Detection of PAP via *the Glu-MSNs@MnO_2 nanocomposites*

In order to investigate the detection capability of the nanoprobes Glu-MSNs@MnO_2, 20 μL of different concentrations of PAP solution was added into 180 μL of the Glu-MSNs@MnO_2 detection system, respectively, and the final concentration of PAP in detection process was kept as 0, 10 μM, 20 μM, 50 μM, 100 μM, 200 μM, 400 μM, 500 μM, 1 mM, and 2 mM. After reacting for 6.5 min, the signal of the detection system was directly read out by PGM. All experiments are repeated at least three times.

Performance of PAP assays in real samples

River water.

Five hundred milliliters of river water was taken from Junzi Lake (Nanjing, China) and filtered to remove impurities by 0.22-μm filter membrane. The prepared PAP solution was added to 1 mL of river water to obtain samples with final concentrations of 30 μM, 80 μM, and 150 μM PAP.

Soil samples.

Soil samples were collected in Nanjing, China, and sieved through an 80-mesh sieve after natural air-drying. The soil was mixed with pure water at a ratio of 1:10 and sonicated for 1 h to allow sufficient dispersion. Then, the mixture was shaken overnight and the suspension was removed to obtain a dark yellow supernatant with pH 7.0 and conductivity 245 μS cm^{-1} for further experiments. The prepared PAP solution was added to 1 mL of the prepared soil samples to obtain samples with final concentrations of 30 μM, 80 μM, and 150 μM PAP.

After the preparation of real samples, the performance of Glu-MSNs@MnO_2 nanoprobes in real samples was tested following the above detection procedure. The only difference was substituting the PAP solution with a series of real samples.

Results and discussion

Characterization of the Glu-MSNs@MnO_2 nanomaterials

The transmission electron microscope (TEM) image revealed that the as-prepared MSNs were highly monodispersed and spherical with a uniform diameter of ~ 100 nm (Fig. 1a), and the HRTEM image and the N_2 adsorption–desorption isotherm analysis demonstrated that the MSNs owned well-ordered porous structures with high specific surface areas 924 $m^2 \cdot g^{-1}$, pore volume 0.886 $cm^3\ g^{-1}$, and a narrow pore-size distribution with the average diameter of 2.84 nm. After loading process, the surface area and pore volume of Glu-MSNs were significantly reduced to 425 $m^2 \cdot g^{-1}$ and 0.287 $cm^3\ g^{-1}$, indicating a noticeable amount of glucose molecules was loaded into the pores (inset of Fig. 1a; Fig. S1). After in situ assembly of the outer layer, the rough surface MnO_2 was around the core MSNs, and the synthesized Glu-MSNs@MnO_2 nanomaterials possessed a well-defined hybrid structure (Fig. 1b). The corresponding scanning TEM (STEM)-energy-dispersive system (EDS) line spectrum and chemical maps confirmed the coexistence of Mn, Si, and O elements (Fig. 1c; Fig. S2). Furthermore, XPS characterization was performed to investigate the composition and valence state; the results of XPS scan spectrum confirmed that the nanomaterials contained Mn (Mn 2p), Si, and O (Fig. 1d). As shown in the Mn 2p spectrum, two binding energies at 653.4 eV and 641.9 eV were consistent with metallic Mn $2p_{1/2}$ and Mn $2p_{3/2}$, respectively. In addition, the spin-energy separation of 11.5 eV indicated that the chemical state of Mn in the nanomaterials was tetravalent (Fig. 1e). And the XRD pattern of the Glu-MSNs@MnO_2 nanomaterials demonstrated that four diffraction peaks at 12.5°, 25.2°, 36.2°, and 65.6° of the nanomaterials correspond to (001), (002), (110), and (020) reflections, respectively, which were consistent with the previous report [35]. All results demonstrated the successful fabrication of Glu-MSNs@MnO_2 nanomaterials.

The stability of the nanoprobes

In order to obtain the best detection performance, the loading capability and stability of the Glu-MSNs@MnO_2 were firstly investigated. Based on the measurements of PGM, the loading quantity of glucose molecules in the MSNs was calculated to be approximately 1.95 mmol g^{-1} MSNs, which was comparable to the previous reported work in the term of loading efficiency [36]. And the results showed that in the absence of target PAP, slight PGM signal change was observed even incubated after 24 h (nearly 0.6) (Fig. S3), indicating that negligible entrapped glucose molecule was released and the Glu-MSNs@MnO_2 nanoprobes owned excellent stability. While adding the target PAP to the detection system, the outcomes was completely different. Just adding 200 μM PAP, significant PGM signal change was observed; the signal increased sharply and reached the maximum at 6.5 min. All the results revealed that the

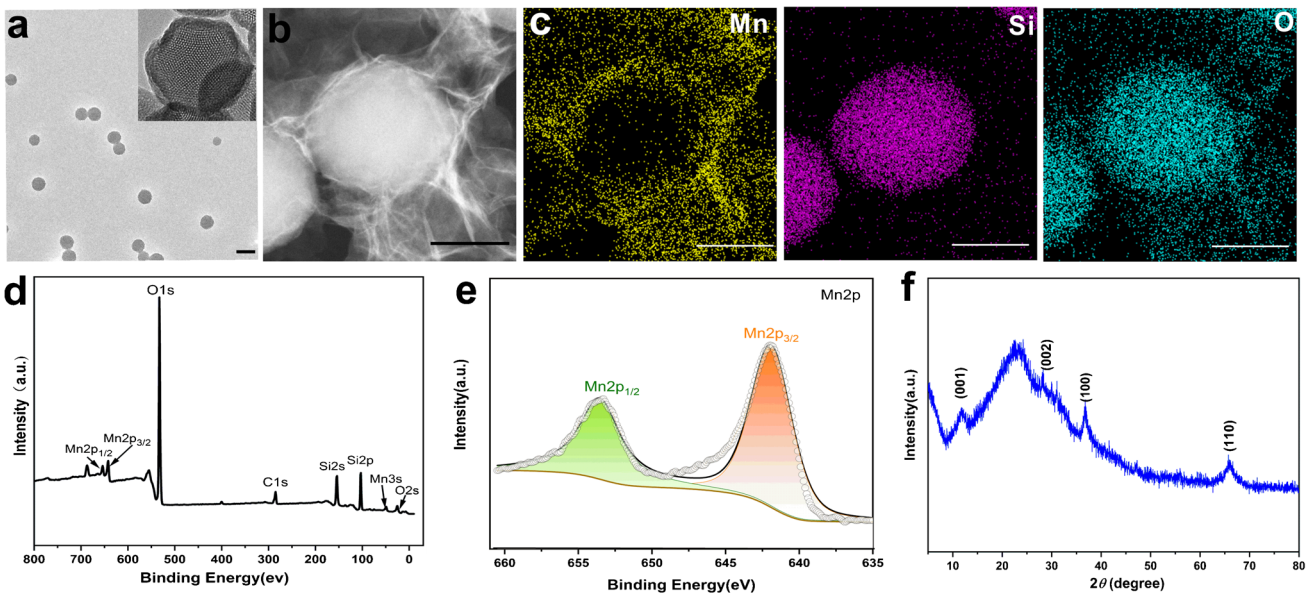

Fig. 1 **a** TEM image of MSNs and HRTEM image of MSNs (inset). **b** TEM image of the Glu-MSNs@MnO_2 nanocomposites. **c** STEM–EDS chemical element mapping of the Glu-MSNs@MnO_2 nanocomposites. Scale bar, 100 nm. Total XPS spectrum (**d**), high-resolution Mn 2p XPS spectrum (**e**), and XRD pattern (**f**) of the Glu-MSNs@MnO_2 nanocomposites

Glu-MSNs@MnO_2 nanoprobes can successfully react with the target PAP, further induce the degradation of outer MnO_2 and the remarkable release of glucose molecule, and then generate significant PGM signal, which verified the detection capability of Glu-MSNs@MnO_2 nanoprobes. Meanwhile, the PGM signal raised up to the maximum at 6.5 min and then reached the plateau; therefore, 6.5 min was chosen as the optimal reaction time for further experiments (Fig. 2a). Moreover, a long-time test was performed to investigate the detection ability of Glu-MSNs@MnO_2 nanoprobes; the outcomes demonstrated that the nanoprobes owned excellent stability and target-response capability even after stored 2 weeks (Fig. 2b). All these corroborated that the prepared Glu-MSNs@MnO_2 nanoprobes owned excellent performance stability for the on-site monitoring of PAP.

Detection capability of Glu-MSNs@MnO_2 nanoprobes

Based on the optimal experimental conditions, the detection performance of Glu-MSNs@MnO_2 nanoprobe for PAP was investigated. As can be seen in Fig. 3a and Fig. S4, with the increment of the concentration of PAP, the PGM signal showed a gradual increase, which indicated that the reaction between PAP and the outer layer MnO_2 successfully induced the degradation of the locker layer of the Glu-MSNs@MnO_2 nanoprobe, then triggered the unlocking process and the release of entrapped glucose, and achieved "one to many" signal output. And the PGM signal of detection system exhibited a linear correlation to the concentration of PAP in the range of 10–400 μM (Fig. 3b), with a linear regression equation $Y=(0.269\pm0.172)+(0.070\pm9.14\times10^{-4})\times$ (μM) ($R^2=0.9992$), and the detection limit was calculated as 2.78 μM according to 3σ/slope, where Y is the PGM signal and X is the PAP concentration. Moreover, the effect of temperature and pH on the detection capability of Glu-MSNs@MnO_2 nanoprobes was investigated, and the results demonstrated that the temperature and pH factor have slight effect on the PGM signal change of the detection system (Fig. S5). All results demonstrated that the amplifiable nanoprobes Glu-MSNs@MnO_2 owned excellent performance for sensitive detection of trace PAP.

The selectivity test

The selectivity test was performed to determine whether the Glu-MSNs@MnO_2 nanoprobes own high specificity for PAP detection in complex environment condition. Similar benzene systems such as 4-aminobenzenesulfonic acid, 4-aminobenzoic acid, diphenylamine, and N-phenyl-1-naphthylamine were selected as analogs to investigate

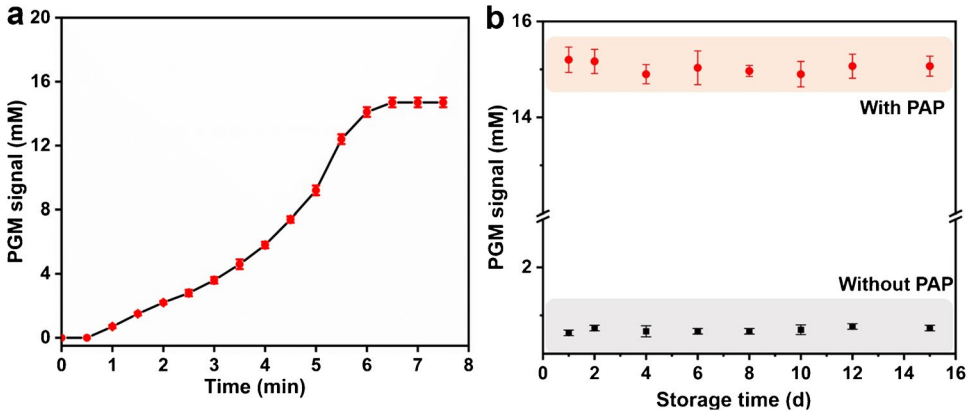

Fig. 2 **a** The PGM signal change of Glu-MSNs@MnO_2 nanoprobe in the presence of PAP (200 μM) with the reaction time prolonging. **b** At a series of storage time points, the PGM signal of the Glu-MSNs@MnO_2 nanoprobe (black symbol) and reacted with 200 μM PAP (red symbol)

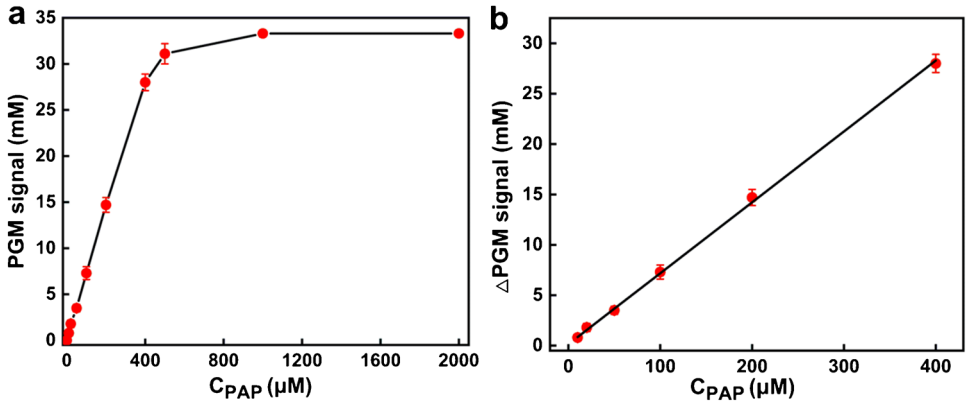

Fig. 3 **a** The PGM signal of the Glu-MSNs@MnO_2 nanoprobes after adding different concentrations of targets PAP (0, 10 μM, 20 μM, 50 μM, 100 μM, 200 μM, 400 μM, 500 μM, 1 mM, 2 mM). **b** The linear relationship of PGM signal to target concentrations of PAP

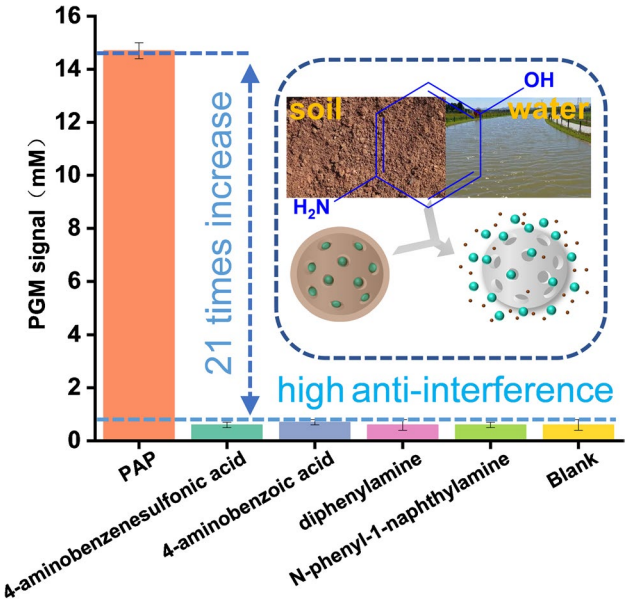

Fig. 4 Selectivity test. PGM signal of the Glu-MSNs@MnO_2 nanoprobes reacting with target PAP (200 μM) and other analogues (1 mM)

the selectivity of the nanoprobes. As shown in Fig. 4, even added a higher concentration of analogue to the Glu-MSNs@MnO_2 detection system, no significant PGM signal change was observed. While added with 200 μM PAP, a remarkable signal increase was observed, and the PGM signal was nearly 21 times higher than that of analogs detection. Moreover, in order to verify the selectivity of our method in environmental samples, several types of inorganic substances such as monovalent cations (K^+, Na^+, NH_4^+) and divalent cations (Mn^{2+}, Ca^{2+}) were utilized for the selectivity test. As shown in Fig. S6, only target PAP induced a significant PGM signal change; conversely, there was negligible PGM signal change in the presence of other inorganic substances. All results indicated that the Glu-MSNs@MnO_2 nanoprobes own good selectivity and can act as excellent candidate for on-site detection of PAP.

Real sample assays

In order to investigate the applicability of the Glu-MSNs@MnO_2 nanoprobes, the recovery tests of water and soil samples were performed. Specifically, different concentrations of PAP were spiked in river water and soil samples to obtain final PAP concentrations of 30.0 μM, 80.0 μM, and 150 μM, respectively. Then, these real samples were analyzed by the Glu-MSNs@MnO_2 nanoprobes. As can be seen in Table 1, the recovery rates were up to 98.8 ± 1.77–101 ± 4.77% in river samples and also up to 96.7 ± 4.83–98.6 ± 2.02% in soil samples. Moreover, in order to further prove that the Glu-MSNs@MnO_2 nanoprobes can be used to detect PAP in complex environmental samples, a real sample was detected by the commonly used quantitative technology UV–Vis quantitative analysis and the proposed method simultaneously. The results revealed that the accuracy of the designed method showed good agreement with that of the UV–Vis quantitative analysis (Fig. S7). And compared with other detection methods, the outcomes revealed that the proposed strategy owned comparable sensitivity, easier operation and faster detection time (Table S1). All results indicated that the Glu-MSNs@MnO_2 nanoprobes own excellent stability in complex environment and possess a promising application for sensitive detection of the environmental pollutants.

Conclusions

We designed and fabricated a one-target-many-trigger signal model sensing strategy for rapid and sensitive detection of the pollutant via the amplifiable nanoprobe Glu-MSNs@MnO_2. Compared to conventional pollutant detection methods, this new strategy possesses several distinct advantages. First, attributed to the high loading capability of MSNs, "one-to-many" signal response model is achieved, which means that very small amount of target PAP can induce the release of a large amounts of signal molecules. Thus, significant signal amplification and highly sensitive detection of PAP are realized. Second, due to the quick response of the locker layer MnO_2 to the target PAP, the whole analysis

Table 1 Recovery tests of PAP spiked in soil and river water sample via the Glu-MSNs@MnO_2 nanoprobes

Samples	Added/(μM)	Measured/(μM)	Recovery/(%)	RSD (n = 3, %)
River water	0	< LOD	-	-
	30.0	30.4	101	4.77
	80.0	79.0	98.8	1.77
	150	151	101	0.95
Soil	0	< LOD	-	-
	30.0	29.0	96.7	4.83
	80.0	77.6	97.0	3.60
	150	148	98.6	2.02

process was rapid; it just needed 6.5 min, which is beneficial for on-site environmental detection. Third, any commercial PGM can be employed as the signal readout in this method, significantly decreasing the cost and the difficulty of operation and increasing the portability and application of such nanoprobes. Therefore, the unique features of the amplifiable nanoprobe Glu-MSNs@MnO_2 make the proposed strategy owns promising potential to achieve rapid, portable, and sensitive on-site detection of aromatic pollutants.

Supplementary Information The online version contains supplementary material available at https://doi.org/10.1007/s00604-024-06204-8.

Author contribution Xiang-Ling Li: conceptualization; methodology; formal analysis; investigation; writing—original draft; visualization. Lei Zhao: investigation; writing—review and editing. Zi-Heng Wang: validation; writing—review and editing. Tian-shun Song: writing—review and editing. Ting Guo: conceptualization; writing—review and editing. Jing Jing Xie: conceptualization; project administration; funding acquisition; supervision.

Funding This work was supported by the National Key Research and Development Program of China (2018YFA0901300), the National Natural Science Foundation of China (Grant No. 22078149), the Natural Science Foundation of Jiangsu Province (No. BK20220002), and the Key Research and Development Program of Jiangsu Province (No. BE2023360).

the National Key Research and Development Program of China,2018YFA0901300,Jing jing Xie,National Natural Science Foundation of China,22078149,Jing jing Xie,Natural Science Foundation of Jiangsu Province,BK20220002,Jing jing Xie,Jiangsu Provincial Key Research and Development Program,BE2023360,Jing jing Xie

Data availability The authors declare that all data generated or analysed during this study are included in this published article (and its supplementary information files).

Declarations

Conflict of interest The authors declare no competing interests.

References

1. Wang CC, Wang W, Wang J, Zhang PP, Miao SD, Jin B, Li LN (2020) Effective removal of aromatic pollutants via adsorption and photocatalysis of porous organic frameworks. RSC Adv 10(53):32016–32019. https://doi.org/10.1039/d0ra05724j
2. Wang Y, Hu DF, Zhang ZX, Yao JM, Militky J, Wiener J, Zhu GC, Zhang GQ (2021) Fabrication of manganese oxide/PTFE hollow fiber membrane and its catalytic degradation of phenol. Materials 14(13):365. https://doi.org/10.3390/ma14133651
3. Benavente R, Lopez-Tejedor D, Perez-Rizquez C, Palomo JM (2018) Ultra-fast degradation of p-aminophenol by a nanostructured iron catalyst. Molecules 23(9):166. https://doi.org/10.3390/molecules23092166
4. Shaban SM, Moon BS, Kim DH (2021) Selective and sensitive colorimetric detection of p-aminophenol in human urine and paracetamol drugs based on seed-mediated growth of silver nanoparticles. Environ Technol Innov 22:101517. https://doi.org/10.1016/j.eti.2021.101517
5. Liu Y, Sheng Y, Yin YC, Ren JA, Lin XR, Zou XJ, Wang XG, Lu XG (2022) Phosphorus-doped activated coconut shell carbon-anchored highly dispersed Pt for the chemoselective hydrogenation of nitrobenzene to p-aminophenol. ACS Omega 7(13):11217–11225. https://doi.org/10.1021/acsomega.2c00093
6. Li M, Ding CP, Jia PD, Guo LH, Wang S, Guo ZY, Su FM, Huang YJ (2021) Semi-quantitative detection of p-aminophenol in real samples with colorfully naked-eye assay. Sens Actuator B-Chem 334:129604. https://doi.org/10.1016/j.snb.2021.129604
7. Santos L, Paiga P, Araujo AN, Pena A, Delerue-Matos C, Montenegro M (2013) Development of a simple analytical method for the simultaneous determination of paracetamol, paracetamol-glucuronide and p-aminophenol in river water. J Chromatogr B 930:75–81. https://doi.org/10.1016/j.jchromb.2013.04.032
8. Tanada N, Kageura M, Hara K, Hieda Y, Takamoto M, Kashimura S (1991) Identification of human hair stained with oxidation hair dyes by gas chromatographic-mass spectrometric analysis. Forensic Sci Int 52(1):5–11. https://doi.org/10.1016/0379-0738(91)90090-6
9. Feng YF, Li YG, Yu SY, Yang QR, Tong YB, Ye BC (2021) Electrochemical sensor based on N-doped carbon dots decorated with manganese oxide nanospheres for simultaneous detection of p-aminophenol and paracetamol. Analyst 146(16):5135–5142. https://doi.org/10.1039/d1an00966d
10. Guan HA, Zhang Y, Liu SP (2022) A novel enhanced electrochemical sensor based on the peroxidase-like activity of Fe_3O_4@Au/MOF for the detection of p-aminophenol. J Appl Electrochem 52(6):989–1002. https://doi.org/10.1007/s10800-022-01684-z
11. Narouie S, Rounaghi GH, Saravani H, Shahbakhsh M (2022) Iodine/iodide-doped polymeric nanospheres for simultaneous voltammetric detection of p-aminophenol, phenol, and; nitrophenol. Microchim Acta 189(8):267. https://doi.org/10.1007/s00604-022-05361-y
12. Xiao Y, Wang K, Yu X-D, Xu J-J, Chen H-Y (2007) Separation of aminophenol isomers in polyelectrolyte multilayers modified PDMS microchip. Talanta 72:1316–1321. https://doi.org/10.1016/j.talanta.2007.01.037
13. Zhao JJ, Liu PY, Song LJ, Zhang L, Liu ZL, Wang YQ (2021) A water stable Eu(iii)-organic framework as a recyclable multi-responsive luminescent sensor for efficient detection of p-aminophenol in simulated urine, and Mn-VII and Cr-VI anions in aqueous solutions. Dalton Trans 50(15):5236–5243. https://doi.org/10.1039/d1dt00112d
14. Lu XL, Wei FD, Xu GH, Wu YZ, Yang J, Hu Q (2017) Surface molecular imprinting on silica-coated CdTe quantum dots for selective and sensitive fluorescence detection of p-aminophenol in water. J Fluoresc 27(1):181–189. https://doi.org/10.1007/s10895-016-1944-7
15. Alatawi H, Hogan A, Albalawi I, O'Sullivan-Carroll E, Wang YN, Moore E (2022) Fast determination of paracetamol and its hydrolytic degradation product p-aminophenol by capillary and microchip electrophoresis with contactless conductivity detection. Electrophoresis 43(7–8):857–864. https://doi.org/10.1002/elps.202100347
16. Zhang XN, Huang XY, Wang ZL, Zhang Y, Huang XW, Li ZH, Daglia M, Xiao JB, Shi JY, Zou XB (2022) Bioinspired nanozyme enabling glucometer readout for portable monitoring of pesticide under resource-scarce environments. Chem Eng J 429:132243. https://doi.org/10.1016/j.cej.2021.132243
17. Zhang H, Gong ZM, Li Y, Yang FQ (2022) A simple and green method for direct determination of hydrogen peroxide and hypochlorite in household disinfectants based on personal glucose meter. Enzyme Microb Technol 155:109996. https://doi.org/10.1016/j.enzmictec.2022.109996
18. Li F, Li XX, Zhu NW, Li RH, Kang HB, Zhang QP (2020) An aptasensor for the detection of ampicillin in milk using a personal

glucose meter. Anal Methods 12(26):3376–3381. https://doi.org/10.1039/d0ay00256a
19. Liu JJ, Geng ZX, Fan ZY, Liu J, Chen HD (2019) Point-of-care testing based on smartphone: the current state-of-the-art (2017–2018). Biosens Bioelectron 132:17–37. https://doi.org/10.1016/j.bios.2019.01.068
20. He F, Wang HJ, Du PF, Li TF, Wang WT, Tan TY, Liu YB, Ma YL, Wang YS, Abd El-Aty AM (2023) Personal glucose meters coupled with signal amplification technologies for quantitative detection of non-glucose targets: recent progress and challenges in food safety hazards analysis. J Pharm Anal 13(3):223–238. https://doi.org/10.1016/j.jpha.2023.02.005
21. Xiang Y, Lu Y (2013) An invasive DNA approach toward a general method for portable quantification of metal ions using a personal glucose meter. Chem Commun 49(6):585–587. https://doi.org/10.1039/c2cc37156a
22. Huang XT, Li JW, Lu M, Zhang WN, Xu ZM, Yu BY, Tian JW (2020) Point-of-care testing of microRNA based on personal glucose meter and dual signal amplification to evaluate drug-induced kidney injury. Anal Chim Acta 1112:72–79. https://doi.org/10.1016/j.aca.2020.03.051
23. Shan YK, Zhang Y, Kang WJ, Wang B, Li JH, Wu XP, Wang SY, Liu F (2019) Quantitative and selective DNA detection with portable personal glucose meter using loo;based DNA competitive hybridization strategy. Sens Actuator B-Chem 282:197–203. https://doi.org/10.1016/j.snb.2018.11.062
24. Ma WX, Liu MH, Xie SP, Liu B, Jiang LZ, Zhang XR, Yuan XY (2022) CRISPR/Cas12a system responsive DNA hydrogel for label-free detection of non-glucose targets with a portable personal glucose meter. Anal Chim Acta 1231:340439. https://doi.org/10.1016/j.aca.2022.340439
25. Cui YL, Zhao QY, Wang CQ, Jiao BN, He Y, Liu HR, Xie LYZ, Wang YW, Liu YL, Fu RJ (2023) Construction of a portable immunosensor for the sensitive detection of carbendazim in agricultural products using a personal glucose meter. Food Chem 407:135161. https://doi.org/10.1016/j.foodchem.2022.135161
26. Kwon D, Lee H, Yoo H, Hwang J, Lee D, Jeon S (2018) Facile method for enrofloxacin detection in milk using a personal glucose meter. Sens Actuator B-Chem 254:935–939. https://doi.org/10.1016/j.snb.2017.07.118
27. Cao YZ, Mo FY, Liu YH, Liu Y, Li GP, Yu WQ, Liu XQ (2022) Portable and sensitive detection of non-glucose target by enzyme-encapsulated metal-organic-framework using personal glucose meter. Biosens Bioelectron 198:113819. https://doi.org/10.1016/j.bios.2021.113819
28. Yang WX, Lu XH, Wang YC, Sun SJ, Liu CH, Li ZP (2015) Portable and sensitive detection of protein kinase activity by using commercial personal glucose meter. Sens Actuator B-Chem 210:508–512. https://doi.org/10.1016/j.snb.2015.01.027
29. Gao X, Li XY, Sun XZ, Zhang JY, Zhao YC, Liu XJ, Li F (2020) DNA tetrahedra-cross-linked hydrogel functionalized paper for onsite analysis of DNA methyltransferase activity using a personal glucose meter. Anal Chem 92(6):4592–4599. https://doi.org/10.1021/acs.analchem.0c00018
30. Xu CN, Lin M, Wang TY, Yao ZL, Zhang WQ, Feng XJ (2022) Colorimetric aptasensor for on-site detection of acetamiprid with hybridization chain reaction-assisted amplification and smartphone readout strategy. Food Control 137:108934. https://doi.org/10.1016/j.foodcont.2022.108934
31. Zhang MY, Ye J, He JS, Zhang F, Ping JF, Qian C, Wu J (2020) Visual detection for nucleic acid-based techniques as potential on-site detection methods A review. Anal Chim Acta 1099:1–15. https://doi.org/10.1016/j.aca.2019.11.056
32. Zhou YB, Yang S, Xiao Y, Zou Z, Qing ZH, Liu JW, Yang RH (2019) Cytoplasmic protein-powered in situ fluorescence amplification for intracellular assay of low-abundance analyte. Anal Chem 91(23):15179–15186. https://doi.org/10.1021/acs.analchem.9b03980
33. Wang J, Li XL, Chen HY, Xu JJ (2020) "Loading-type" plasmonic nanoparticles for detection of peroxynitrite in living cells. Anal Chem 92(23):15647–15654. https://doi.org/10.1021/acs.analchem.0c04017
34. Lu LL, Zhang Q, Gu Y, Li XL, Xie JJ (2022) Core-shell "loading-type" nanomaterials towards: simultaneous imaging analysis of glutathione and microRNA. Anal Chim Acta 1196:339551. https://doi.org/10.1016/j.aca.2022.339551
35. Yuan DS, Zhang T, Guo Q, Qiu FX, Yang DY, Ou ZP (2017) A novel hierarchical hollow SiO2@MnO2 cubes reinforced elastic polyurethane foam for the highly efficient removal of oil from water. Chem Eng J 327:539. https://doi.org/10.1016/j.cej.2017.06.144
36. Fu LB, Zhuang JY, Lai WQ, Que XH, Lu MH, Tang DP (2013) Portable and quantitative monitoring of heavy metal ions using DNAzyme-capped mesoporous silica nanoparticles with a glucometer readout. J Mater Chem B 1:6123. https://doi.org/10.1039/c3tb21155j